ELSEVIER

Contents lists available at ScienceDirect

## Journal of the European Ceramic Society

journal homepage: www.elsevier.com/locate/jeurceramsoc





# Densification of the entropy stabilized oxide (Mg<sub>0.2</sub>Co<sub>0.2</sub>Ni<sub>0.2</sub>Cu<sub>0.2</sub>Zn<sub>0.2</sub>)O

V. Jacobson<sup>a,b</sup>, K. Gann<sup>b</sup>, M. Sanders<sup>b</sup>, G. Brennecka<sup>b,\*</sup>

- <sup>a</sup> National Renewable Energy Laboratory, 16000 Denver West Parkway, Golden, CO, USA
- <sup>b</sup> Colorado School of Mines, 1500 Illinois Ave., Golden, CO, USA

ARTICLE INFO

Keywords: Entropy Oxide Mixing Thermal profile

#### ABSTRACT

The first entropy-stabilized oxide,  $(Mg_{0.2}Co_{0.2}Ni_{0.2}Cu_{0.2}Zn_{0.2})O$ , was reported in 2015. Initial studies synthesized this material using solid state processing and were limited to densities < 80%. Here, we report a straightforward solid state route to sinter samples to densities up to 98% of the theoretical by identifying the role of oxygen and promoting the resulting mechanisms in densification. Previous works have studied effects of cation stoichiometry on the entropy-driven reaction to form a single phase, but few have explored the associated effects of anion stoichiometry and/or redox chemistry on both phase stability and densification. We demonstrate here that tuning heating rate and  $pO_2$  during heating of initially-homogeneous calcined powders can enhance densifying diffusion processes and enable reliable sintering of dense  $Mg_{0.2}Co_{0.2}Ni_{0.2}Cu_{0.2}Zn_{0.2}O$ 0 samples.

## 1. Introduction

The first entropy-stabilized oxide (ESO), (Mg<sub>0.2</sub>Co<sub>0.2</sub>Ni<sub>0.2</sub>Cu<sub>0.2</sub>Zn<sub>0.2</sub>) O, was reported in 2015 by Rost et al. [1]. This system is commonly referred to as J14 and will be referred to as such in the remainder of this study. Although many other high-entropy ceramics (of which ESOs are a subset) have been reported since [2–5,6,7], this five-cation system remains the most studied. Above 875 °C, J14 is stable in a single-phase rock salt structure with a homogeneous distribution of cations. Both the structure and the cation distribution are maintained upon quenching to room temperature [1,8]. Some lattice distortion has been observed in these samples and has been explained both by local distortions in the oxygen anion sublattice that accommodates the differently sized cations and by Jahn-Teller distortions, particularly those associated with the  $Cu^{2+}$  cations [8–11,12,13]. Both rapid Li-ion conduction [4,14–16] and high redox activity [17] have been reported for J14 and its derivatives, highlighting the importance of ionic mobility and redox reactions in this system. While characterization of single phase samples has been well explored, a fundamental understanding of densification and sintering in this flagship ESO system is still lacking.

The majority of prior studies on J14 utilized bulk ceramic processing by mixed-oxide and carbonate approaches and were unable to achieve densities greater than 80% of the theoretical density [1,4,12,18,19] whether by sintering calcined powders or using a reactive sintering approach from the raw precursors [3]. Reaction-assisted flash sintering methods have also been used to synthesize single-phase J14 in a matter

of seconds at room temperature; however, the reported densities are less than 62% of the theoretical density [3]. In 2018, Biesuz et al. [20] leveraged the fine particle sizes and intimate cation mixing of hydrothermally-prepared and co-precipitated powders to prepare sintered samples of 91% and 97% densities, respectively. Additionally, Hong et al. [9] produced 99.3% dense samples using field-assisted sintering, with a heating rate of 100 °C min<sup>-1</sup> and simultaneous application of 35 MPa of uniaxial pressure. These studies achieved high density sintered samples but provided limited mechanistic insight for why their routes had succeeded where others had failed.

The original studies from Rost et al. [1,8] confirmed the entropy-stabilized (and not simply 'high-entropy') aspects of this composition by demonstrating that the phase transition between the constituent oxides and the single-phase homogeneous rock salt is both reversible and endothermic. The temperature of the entropy-stabilized transition is roughly 875 °C for the equimolar version of this chemistry. Note that because this single phase is stabilized by entropy, its apparent stability at room temperature relies on kinetic hindrance; thus, quenched samples stay homogeneous, but CuO can precipitate during slow cooling [21]. Likewise, during slow heating- commonly used during traditional sintering- samples experience finite time at temperatures where phase separation is both energetically favorable and kinetically feasible. Further, some studies have noted that Co<sup>2+</sup> cations oxidize to Co<sup>3+</sup> during heating [13,20,22], which would be incompatible with the homogeneous distribution of divalent cations in a rock salt lattice and therefore add an enthalpic driving force for cation diffusion.

E-mail address: gbrennec@mines.edu (G. Brennecka).

<sup>\*</sup> Corresponding author.

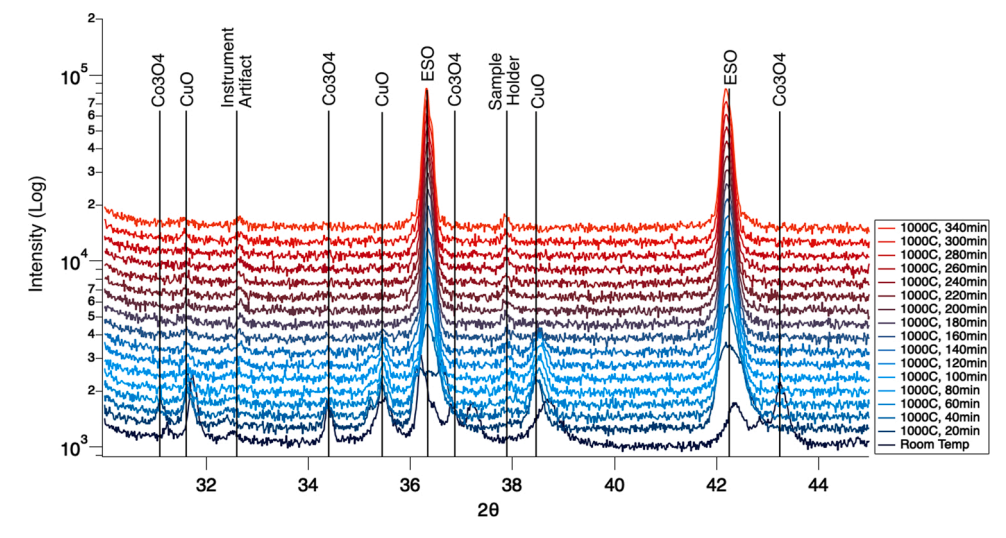


**Fig. 1.** Precursor binary oxides were mixed and then measured using a hot stage in-situ XRD. A heating rate of 500 °C min<sup>-1</sup> to 1000 °C followed by a 6 h hold reveals that approximately 5.6 h at temperature is required for full incorporation of all precursor phases into the single phase rock salt J14. All subsequent tests were conducted on this single phase powder.

We hypothesize that such transient reactions can strongly affect diffusion rates and therefore impact the dominant sintering mechanism at any given stage of sintering. Here, we show that designing a thermal profile around known reactions can facilitate densification to > 98% theoretical density in the flagship entropy-stabilized oxide J14 ceramics fabricated from calcined powders.

## 2. Experimental details

Stoichiometric (Mg<sub>0.2</sub>Co<sub>0.2</sub>Ni<sub>0.2</sub>Cu<sub>0.2</sub>Zn<sub>0.2</sub>)O was fabricated by mixing equimolar amounts of MgO [Alfa Aesar, 99.99%], Co(II,III)O [Alfa Aesar, 99.7%], NiO [Sigma Aldrich, 99.995%], CuO [Alfa Aesar, 99.995%], and ZnO [Alfa Aesar, 99.99%]. The Co(II,III)O powder was analyzed via XRD refinement using GSAS II[23] in order to determine the relative amounts of CoO and Co2O3 in order to ensure proper, equimolar batching of the cations. These were either roller milled for more than 6 h or planetary milled for 2 h in ethanol with yttrium-stabilized zirconia (YSZ) milling media and fish oil as a dispersant. After milling, the powder was calcined in air at 900 °C for 8 h and quenched in air. The calcined powder was milled in a planetary mill, using the same parameters, to reduce the particle size. The milled powder suspension was dried overnight to evaporate the ethanol. The dried powder was mixed using a mortar and pestle to combat flocculation and size segregation during drying. Particle sizes and size distribution were analyzed by a Microtrac S3500 particle size analyzer and SEM image analysis techniques. This single-phase, calcined powder was used for all subsequent sintering experiments.

Cylindrical pellets were formed by pressing the powder in either a 6.35 mm or 12.7 mm diameter die in a uniaxial Carver press. Prior to powder loading, the dies were lubricated with stearic acid dissolved in methanol. Samples were pressed at approximately  $1.25\times10^8$  Pa for at least 5 min. Green density was measured via geometric density measurements, and samples were sintered only if the measured green density was greater than 55% of the theoretical density.

All heat treatments included a double crucible configuration, with an outer alumina crucible and lid to minimize loss of volatile species. A liner of crimped platinum foil prevented direct contact and potential reaction of the J14 powder and pellets with the alumina crucible. Pellets were sintered in either a box furnace or a horizontal tube furnace under the heating profiles and atmospheres detailed in Section 3.3. After sintering, all samples were air quenched by immediate removal of the crucibles from the hot furnace.

To verify entropy stabilization and the single phase development in

both calcined powders and sintered pellets, crystal structure and phase purity were confirmed using a PANalytical PW3040 X-ray Diffractometer (XRD). To better understand the kinetics of the precursor incorporation process, in-situ XRD data were collected using a PANalytical Empyrean XRD with a domed DHS 1100 stage. First, the mixed-powder samples were heated at 500 °C min<sup>-1</sup> to 1000 °C and held at 1000 °C for more than 6 h, and XRD patterns were collected every 20 min. These data were consistent with earlier reports of the reactions of these precursor oxides to form a single rock salt phase that persists upon quenching. To better understand the stability of the rock salt phase upon reheating, additional in-situ XRD tests were run on calcined, singlephase powders using a much slower heating ramp rate of 5 °C min<sup>-1</sup> up to 1100 °C min<sup>-1</sup> in both air and nitrogen atmospheres. Each of these XRD tests used Cu-k<sub>a</sub> radiation and GSAS II for XRD data refinement [24]. Pawley methods were used for refinement of patterns from samples that were clearly a single phase, and a combination of Rietveld and Le Bail methods were used to refine patterns from samples with secondary phases or anisotropic lattice strain. Linear shrinkage was measured with a Netzsch Dilatometer 402. A Netzsch STA 449 F3 ASC Jupiter was used for simultaneous data collection for differential scanning calorimetry (DSC) and thermogravimetric analysis (TGA). Constant-rate heating experiments were conducted at ramp rates between 2 °C min<sup>-1</sup> and 10 °C min<sup>-1</sup> to 1100 °C for each of these thermal analysis techniques.

Porosity and grain size were examined on images collected using an FEI Quanta 600i Environmental Scanning Electron Microscope (ESEM) under high vacuum (<0.75 Torr) with 20 kV accelerating voltage. Prior to imaging, samples were polished to a 1  $\mu$ m diamond grit and thermally etched for at least 90 min at a temperature 50°C below the sintering temperature. The line intercept method [25] was used in conjunction with ImageJ software [26] to find the average grain size. Densities of samples were determined by applying Archimedes' principle and a fluid displacement technique. Calculated densities were verified by the porosity observed in ESEM micrographs.

## 3. Results and discussion

## 3.1. Crystal structure

Diffraction patterns from both single-phase calcined powders and sintered ceramic pellets match the simulated diffraction pattern [27] for a cubic Fm3m rock salt structure with randomly-distributed cations and are consistent with previous reports [8]. Refinements of XRD data for

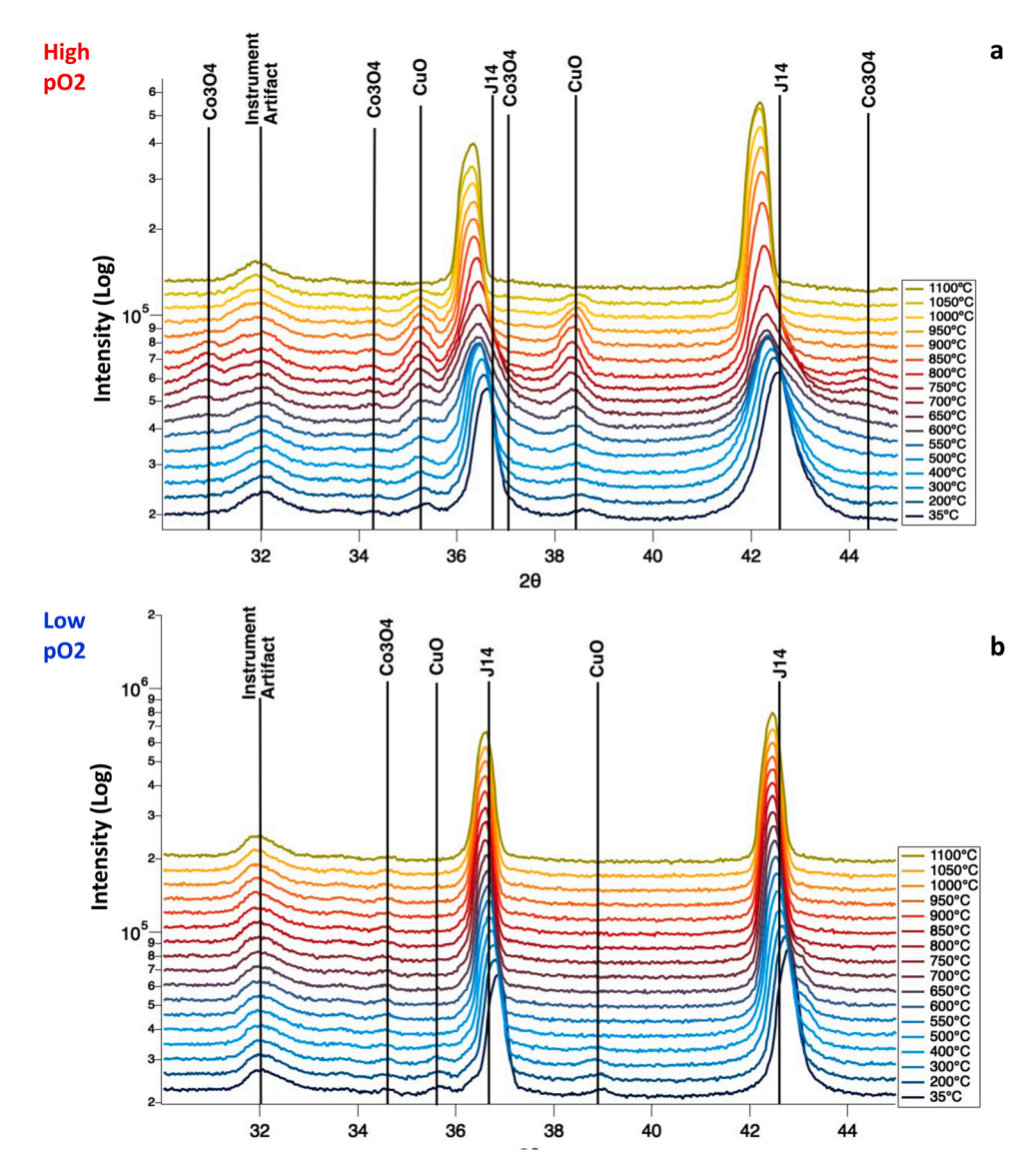


Fig. 2. (a) In-situ XRD performed in air with a heating rate of 5 °C min<sup>-1</sup> shows that, starting around 500°C, both tenorite CuO and spinel  $Co_3O_4$  begin to precipitate from the calcined powder and are fully re-integrated above 1000 °C. (b) The same test run in a nitrogen atmosphere shows the full integration of the precursor powder into a single phase, with some peak broadening around  $2\theta = 43.5^{\circ}$  attributable to Jahn-Teller distortion [12] between 400 °C and 800 °C.

this calcined powder indicate a lattice constant of 4.235Åwith a weighted data residual of 3.6%. After calcination, the powder was roller milled overnight and the maximum particle size was less than 10  $\mu$ m. These XRD data show sharp, symmetric peaks with no evidence of the anisotropic lattice distortions reported previously [12,20].

*In-situ* XRD data collected from a mixture of MgO, Co(II,III)O, NiO, CuO, and ZnO with equimolar amounts of each cation show that all constituent phases incorporated into the single phase rock salt after approximately 5.6 h at 1000 °C (Fig. 1). Consistent with previous findings, the CuO phase is the last phase to incorporate [1]. The length of time required for the single phase to form under isothermal conditions indicates that the entropy-driven transition to a single phase is kinetically limited under these conditions.

The integration of precursors into the single phase has been studied previously, [1,8,20] however open questions remain about the sintering process itself. To probe our hypothesis that the partial pressure of oxygen  $(pO_2)$  can affect atomic diffusion and sample densification, we conducted further hot stage in-situ XRD experiments on the calcined powder, which exhibited a small amount of residual CuO as a result of insufficiently rapid quenching. A 6.35 mm diameter pellet was heated at 5 °C min<sup>-1</sup> in air and measured at the temperature intervals shown in

Fig. 2(a). The results of this in-situ experiment show that both CuO and  ${\rm Co_3O_4}$  begin to precipitate out of the single phase powder around  ${\rm 500^\circ C}$  and persist at least up to  ${\rm 1000^\circ C}$ . No evidence of any phase other than the single rock salt is evident after one-hour at  ${\rm 1100^\circ C}$ . In Fig. 2(b), the same heating profile run in a nitrogen atmosphere shows no secondary phase development and the single phase is fully formed after reaching  ${\rm 1100^\circ C}$ . This demonstrates that secondary phases require some amount of atmospheric oxygen in order to form.

#### 3.2. Thermal analyses

In order to better understand the kinetic effects of the secondary phase development and/or peak broadening shown in Fig. 2, differential scanning calorimetry and thermogravimetry (DSC/TG) measurements were carried out on the calcined, single-phase powders with a heating rate of 5 °C min $^{-1}$  to examine the heat and mass flow associated with the phase transitions. These data are shown in Fig. 3(a) and (b). Between 500 °C and 680 °C in air, Fig. 3(a), there is an exothermic reaction accompanied by a mass gain, followed immediately by an endothermic reaction and mass loss. This thermal behavior has been attributed to the formation of Co<sub>3</sub>O<sub>4</sub> spinel in addition to partial formation of the rock salt

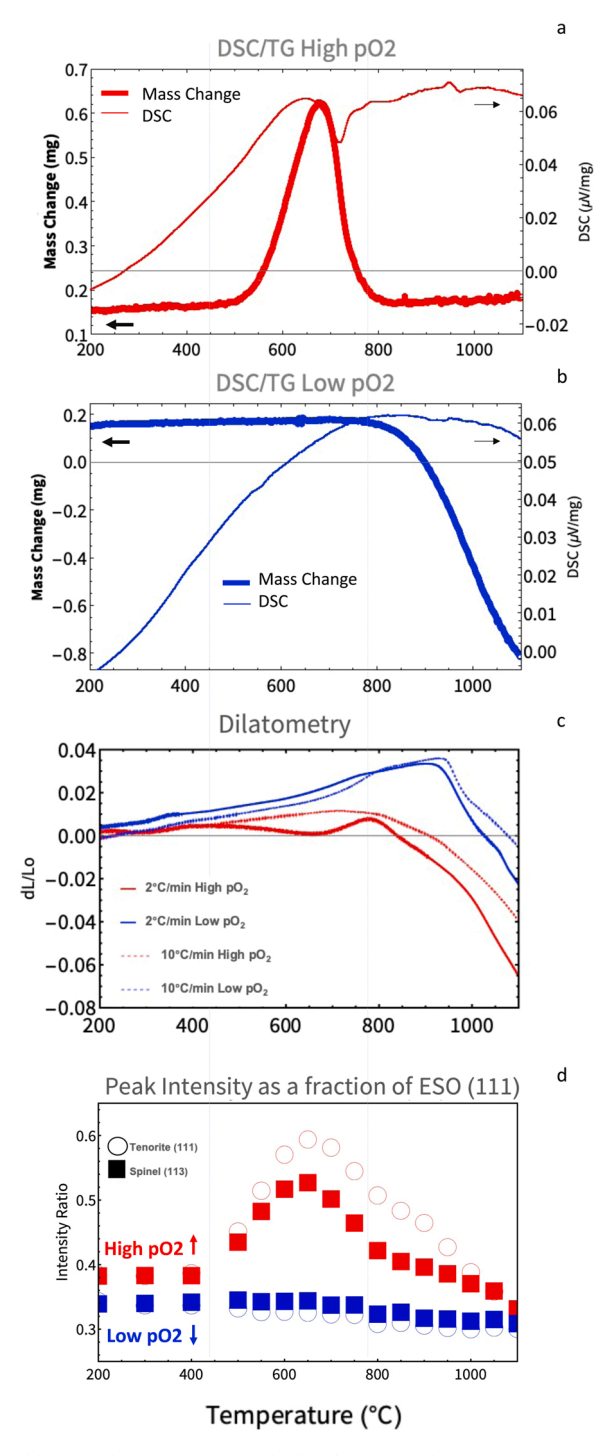


**Fig. 3.** Between 500 °C and 800 °C, chemical and kinetic phenomena occur which indicate that the formation of secondary phases at low heating ramp rates in high  $pO_2$  environments are linked to higher sample densities. (a) DSC-TG analysis of calcined, single phase J14 powders conducted in air show a mass gain and loss from 500 °C to 800 °C. This mass change is complimented by a sharp endothermic dip, indicative of a phase change. In this same temperature range, (b) DSC-TG analysis of calcined, single phase J14 powders conducted in Ar show no evidence of a phase transition prior to the formation of the primary rock salt phase. (c) Dilatometry data were collected using the same powder heated under two different ramp rates and two different atmospheres: 2 °C min<sup>-1</sup> and 5 °C min<sup>-1</sup>, ambient air (high  $pO_2$ ) and Ar (low  $pO_2$ ). Dilatometry in air shows sample compression followed by expansion before the primary onset of densification at 800 °C when slower heating rates are used. Based on these data, it is most probable that secondary phase formation is enhanced by atmospheric oxygen, with high  $pO_2$  and low heating ramp rates. (d) XRD peak ratios of CuO tenorite (111) and  $Co_3O_4$  (113) as a fraction of the J14 rock salt (111) peak from the in-situ XRD shown in Fig. 2(a) indicate the growth and reabsorption of these secondary phases over the same temperature range in high  $pO_2$  atmosphere and the XRD from Fig.2(b) shows that the secondary phases do not precipitate.

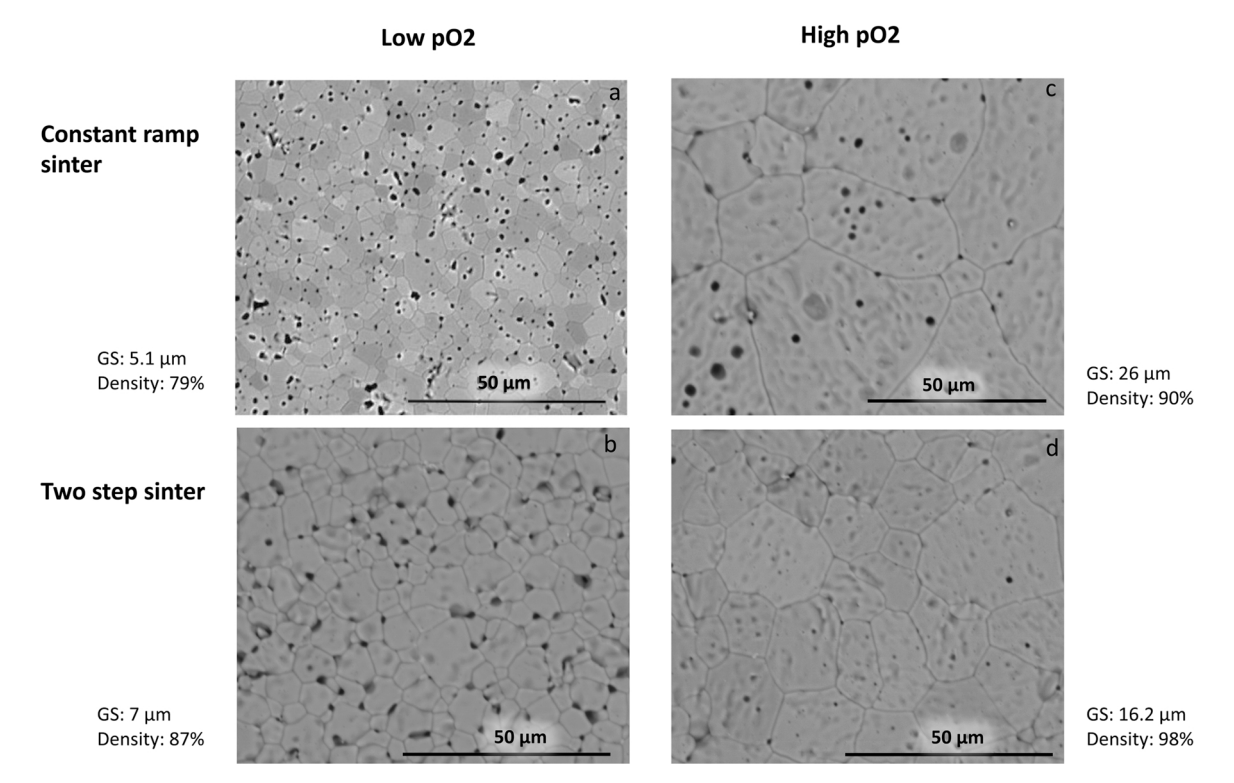


**Fig. 4.** Micrographs of sintered, polished, and thermally etched sample surfaces. GS = average grain size. (a) Sample sintered via a constant heating ramp rate in a low  $pO_2$  atmosphere. Grains are an average of 5.1 μm across, with a large quantity of both trapped intragranular pores and pores on the grain boundaries. (b) Sample prepared via the two step sintering profile in a low  $pO_2$  atmosphere. Grains are approximately 7 μm across with many pores at grain boundaries and triple points. (c) Sample sintered via a constant heating ramp rate in a high  $pO_2$  atmosphere. Grains are an average of 26 μm across, with a large quantity of trapped intragranular pores. (d) Sample sintered via the two step sintering profile in a high  $pO_2$  atmosphere. Grains are an average of 16.2 μ m in diameter and have minimal porosity.

structure, which is consistent with the established order of coalescence for the precursor binary oxides that was shown in previous studies [1,12,20], is confirmed by our data in Fig. 1, and is consistent with the known propensity of Co to exist in a + 3 state under ambient conditions [28]. The mass gain in Fig. 3(a) is associated with the oxidation of CoO to Co<sub>3</sub>O<sub>4</sub>. The endothermic reaction seen in Fig. 3(a) accompanied by a mass loss between 680 °C and 780 °C is likely due to the final formation of the single-phase rock salt and to the loss of oxygen that was incorporated during the preceding formation of Co<sub>3</sub>O<sub>4</sub>. The precipitation of CuO, while verified over a similar temperature range, would not cause a change in mass, though its precipitation and re-absorption may contribute to the endotherm seen at 750 °C. Fig. 3

(b) shows the DSC-TG data collected on the same sample in an Ar atmosphere (low  $pO_2$ ). These data show only a gradual exothermic reaction and mass loss starting around 820°C (most likely associated with the loss of volatile metallic Zn). These thermal behaviors are consistent with formation of the rock salt J14 without secondary phase formation under a low- $pO_2$  atmosphere.

Previous studies have prepared samples via similar solid-state processing methods of milling, heating in a furnace at a constant ramp rate with a dwell at approximately 1000 °C for 12 h, and an air quench to achieve the single phase rock salt structure [1,8,12,16,22]. However, the density of samples synthesized by this process were less than 80% of the theoretical density of J14. We collected dilatometry data from a single-phase, calcined powder sample during heating at two different ramp rates to determine how the ramp rate affected densification and to identify an ideal temperature for isothermal dwells. To investigate the kinetics of secondary phase formation, as seen in Fig. 2, these different heating profiles were run in both oxidizing and reducing atmospheres to encourage and suppress the secondary phase formation, respectively. Dilatometry data indicating sample expansion under these different gas atmospheres are shown in Fig. 3(c).

For each of the thermal profiles investigated in Fig. 3(c), densification inflection points are observed around 800 °C in air and around 950 °C in Ar. In air, there is a dip in the dilatometry profile followed by a peak between 500 °C and 800 °C for the 2 °C min<sup>-1</sup> ramp rate, indicating contraction and resumed expansion before the sample begins final densification. In contrast, the 10 °C min<sup>-1</sup> ramp shows a smooth transition to the primary inflection point at 950 °C. The fact that the dip in the air trace is observed only at the slower ramp rate and not the faster ramp rates indicates that the decrease in volume is kinetically limited. This shrinkage and expansion is likely due to the precipitation of the secondary phases of tenorite CuO and spinel Co<sub>3</sub>O<sub>4</sub>, followed by the reformation of a single-phase rock salt. This dip is not observed in measurements in Ar at either ramp rate, which supports the findings of previous studies and suggests that this effect is associated with the oxidation of Co from 2<sup>+</sup> to 3<sup>+</sup> during the thermal treatment in the oxidizing (air) atmosphere. The ratios of the peaks of the secondary phases (Co<sub>3</sub>O<sub>4</sub> (113) peak at 34.4° and CuO (111) peak at 38.5°) to the J14 (111) peak at 36.7° as a function of temperature from Fig. 2 are shown in Fig. 3(d). This emphasizes that both of these phases precipitate and reabsorb across the same temperature range as both the densification dip indicated by dilatometry (Fig. 3(c)) and the phase change indicated by DSC-TG in an oxygen-rich environment (Fig. 3(a)). This suggests a correlation between molecular oxygen evolution, mass loss, and the endotherm near 750 °C seen in Fig. 3(a). The lack of change shown in Fig. 3(d) for the low pO<sub>2</sub> sample shows that oxygen is critical to this phase evolution.

## 3.3. Heating profiles

Based on the data presented thus far and previous work regarding grain growth mechanisms [29], several thermal profiles and atmospheres were tested for maximum densification. Initially, based on the

previous literature, a simple ramp of 10° min<sup>-1</sup> to 1100 °C in an ambient air environment followed by at least a 10 h hold and air quench was used. The resulting microstructure is shown in Fig. 4(a). This thermal profile produced fairly small grains and achieved a density of about 79%, similar to previous reports. Based on the dilatometry, DSC/TG, and in-situ XRD data, a thermal profile was designed to ramp slowly (5 °C min<sup>-1</sup>) up to 750 °C, the temperature of the onset of densification, and then ramp more quickly (10 °C min<sup>-1</sup>) through the primary densification regime to a final sintering temperature of 1050 °C for at least a 10 h isothermal hold followed by air quenching. This new profile produced slightly larger grains and increased density to 87%. The two-step thermal profile increased densification without excessive coarsening, and most of the remaining porosity is confined to grain boundaries and triple points. Porosity trapped within grains is limited, suggesting that these heating profiles balance grain boundary mobility relative to pore mobility more successfully than sintering with a constant ramp rate. Samples sintered using this two-step heating profile in low pO<sub>2</sub> did not densify beyond 87% of the theoretical density. These densities determined by Archimedes principle are consistent with the micrographs of polished and thermally etched surfaces in Fig. 4(a) and 4(b).

The dilatometry data from Fig. 3(c) indicate that the heating ramp rate dictates whether or not the formation of secondary phases is kinetically favorable. Densification commonly occurs via mass transport from grains into pores, and this process is typically mediated by vacancy diffusion to the grain boundaries from regions close to the pore surface [30]. Based on this understanding, the development of vacancies of the rate limiting species in the sintering process will enhance densification. Transition metal rock salt monoxides frequently accommodate changes in cation oxidation state via the formation of cation vacancies [31]. The equation for equilibrium when oxygen gas is introduced to a rock salt monoxide system is:

$$\frac{1}{2}$$
O<sub>2</sub>(g)  $\leftrightarrow$  O<sub>0</sub><sup>×</sup> +  $V''_{TM}$  +  $2h$ .

The development of cation vacancies resulting from the introduction of gaseous oxygen also includes the secondary phase precipitation of  $Co_3O_4$ , as shown by the equation:

$$\frac{1}{2}O_2(g) + 3CoO \leftrightarrow Co_3O_4$$

where the  $\text{Co}^{2+}$  ion adopts a 3+ charge in concert with the transition to a spinel crystal structure. By this logic, we may use the development of  $\text{Co}_3\text{O}_4$  as an indicator for transition metal vacancies in the rock salt lattice.

In order to create an oxygen-rich sintering environment, 50 sccm of oxygen was added to the open-ended tube furnace used for sintering. Samples fabricated in this high  $pO_2$  atmosphere with a constant ramp rate of 10 °C min<sup>-1</sup> and an isothermal hold at 1050 °C for at least 10 h showed a greatly improved density over those sintered under low  $pO_2$ . The grains are nearly five times larger than in the low  $pO_2$  sample and the density is increased to 90%. Intragranular porosity is evident in these samples, indicating that grain boundary mobility is much higher than pore mobility under this sintering profile (Fig. 4(c)). When the two-step thermal profile was used in a high  $pO_2$  atmosphere, density increased to 98% and intragranular porosity is very limited, indicating a balance between grain boundary and pore mobilities (Fig. 4(d)).

## 4. Conclusions

Bulk single-phase rock salt (Mg $_{0.2}$ Co $_{0.2}$ Ni $_{0.2}$ Cu $_{0.2}$ Zn $_{0.2}$ )O samples can be fabricated with repeatably high density by designing a heating profile based around the kinetics of transient reactions. Sintering in an oxygenrich atmosphere by first heating at a relatively slow ramp rate up to 750 °C and then heating more quickly to the primary sintering temperature of 1050 °C yields samples with at least 98% of the theoretical density. This high density results from  $pO_2$ -mediated secondary phase development, increased vacancy diffusion from areas of grains near pore surfaces into grain boundaries, and re-integration of Co $_3O_4$  spinel and CuO tenorite at high temperatures to form a final single-phase rock salt.

These consistently dense bulk samples will enable higher-fidelity future studies of electrical and mechanical measurements that require low porosity to attain high-quality data.

## **Declaration of Competing Interest**

The authors declare that they have no known competing financial interests or personal relationships that could have appeared to influence the work reported in this paper.

### Acknowledgments

Work at CSM was partially supported by the National Science Foundation (DMR-1555015 and DMREF-1534503). We would like to thank A. Mis for assistance in data processing; M. Papac for editing and process support; K.Steirer for in-situ XRD support; and M. Beuerlein for data collection and support.

#### References

- C.M. Rost, E. Sachet, T. Borman, A. Moballegh, E. Dickey, D. Hou, J. Jones, S. Curtarolo, J. Maria, Entropy-stabilized oxides, Nat. Commun. 6 (2015) 8485, https://doi.org/10.1038/ncomms9485.
- [2] C. Oses, C. Toher, S. Curtarolo, High-entropy ceramics, Nat. Rev. Mater. 5 (4) (2020) 295–309, https://doi.org/10.1038/s41578-019-0170-8.
- [3] D. Liu, X. Peng, J. Liu, L. Chen, Y. Yang, L. An, A. Sarkar, Q. Wang, A. Schiele, M. R. Chellali, S.S. Bhattacharya, D. Wang, T. Brezesinski, H. Hahn, L. Velasco, B. Breitung, J. Liu, G. Shao, D. Liu, K. Chen, K. Wang, B. Ma, K. Ren, Y. Wang, Ultrafast synthesis of entropy-stabilized oxide at room temperature, Adv. Mater. 31 (26) (2020) 2504–2508, https://doi.org/10.1002/adma.201806236.
- [4] A. Sarkar, Q. Wang, A. Schiele, M.R. Chellali, S.S. Bhattacharya, D. Wang, T. Brezesinski, H. Hahn, L. Velasco, B. Breitung, High-entropy oxides: fundamental aspects and electrochemical properties, Adv. Mater. 31 (26) (2019), https://doi. org/10.1002/adma.201806236.
- [5] G. Zhang, Y. Wu, High-entropy transparent ceramics: review of potential candidates and recently studied cases, International J. Appl. Ceram. Technol. (2021), https://doi.org/10.1111/ijac.13856.
- [6] M. Pianassola, M. Loveday, J.W. McMurray, M. Koschan, C.L. Melcher, M. Zhuravleva, Solid-state synthesis of multicomponent equiatomic rare-earth oxides, J. Am. Ceram. Soc. 103 (4) (2020) 2908–2918, https://doi.org/10.1111/ ices.16731.
- [7] S. Zhai, J. Rojas, N. Ahlborg, K. Lim, M.F. Toney, H. Jin, W.C. Chueh, A. Majumdar, The use of poly-cation oxides to lower the temperature of two-step thermochemical water splitting, Energy Environ. Sci. 11 (8) (2018) 2172–2178, https://doi.org/ 10.1033/c8ee00050f
- [8] C. Rost, Z. Rak, D. Brenner, J. Maria, Local structure of the MgxNixCoxCuxZnxO (x=0.2) entropy-stabilized oxide: An EXAFS study, J. Am. Cer. Soc. 100 (6) (2017) 2732–2738, https://doi.org/10.1111/jace.14756.
- [9] W. Hong, F. Chen, Q. Shen, Y. Han, W.G. Fahrenholtz, L. Zhang, Microstructural evolution and mechanical properties of (Mg,Co,Ni,Cu,Zn)O high-entropy ceramics, J. Am. Ceram. Soc. (2018) 1–10, https://doi.org/10.1111/jace.16075, jace.16075, (https://onlinelibrary.wiley.com/doi/abs/10.1111/jace.16075).
- [10] L.K. Bhaskar, V. Nallathambi, R. Kumar, Critical role of cationic local stresses on the stabilization of entropy-stabilized transition metal oxides, J. Am. Ceram. Soc. 103 (5) (2020) 3416–3424, https://doi.org/10.1111/jace.17029.
- [11] Z. Rák, J.P. Maria, D.W. Brenner, Evidence for Jahn-Teller compression in the (Mg Co Ni Cu Zn)O entropy-stabilized oxide: A DFT study, Mater. Lett. 217 (2018) 300–303, https://doi.org/10.1016/j.matlet.2018.01.111.
- [12] D. Berardan, A.K. Meena, S. Franger, C. Herrero, N. Dragoe, Controlled Jahn-teller distortion in (MgCoNiCuZn)O-based high entropy oxides, J. Alloy. Compd. 704 (2017) 693–700, https://doi.org/10.1016/j.jallcom.2017.02.070.
- [13] P.B. Meisenheimer, L.D. Williams, S.H. Sung, J. Gim, P. Shafer, G.N. Kotsonis, J. P. Maria, M. Trassin, R. Hovden, E. Kioupakis, J.T. Heron, Magnetic frustration control through tunable stereochemically driven disorder in entropy-stabilized oxides, Phys. Rev. Mater. 3 (10) (2019) 1–9, https://doi.org/10.1103/PhysRevMaterials.3.104420.
- [14] D. Bérardan, S. Franger, A. Meena, N. Dragoe, Room temperature lithium superionic conductivity in high entropy oxides, J. Mater. Chem. A 4 (24) (2016) 9536–9541, https://doi.org/10.1039/c6ta03249d.
- [15] N. Qiu, H. Chen, Z. Yang, S. Sun, Y. Wang, Y. Cui, A high entropy oxide (Mg<sub>0.2</sub> Co<sub>0.2</sub> Ni<sub>0.2</sub> Cu<sub>0.2</sub> Zn<sub>0.2</sub> O) with superior lithium storage performance, J. Alloy. Compd. 777 (2019) 767–774, https://doi.org/10.1016/j.jallcom.2018.11.049.
- [16] D. Bérardan, S. Franger, D. Dragoe, A.K. Meena, N. Dragoe, Colossal dielectric constant in high entropy oxides, Phys. Status Solidi - Rapid Res. Lett. 10 (4) (2016) 328–333, https://doi.org/10.1002/pssr.201600043.
- [17] S. Zhai, J. Rojas, N. Ahlborg, K. Lim, M.F. Toney, H. Jin, W.C. Chueh, A. Majumdar, The use of poly-cation oxides to lower the temperature of two-step thermochemical water splitting, Energy Environ. Sci. 11 (8) (2018) 2172–2178, https://doi.org/ 10.1039/c8ee00050f.

- [18] Z. Rak, C. Rost, M. Lim, P. Sarker, C. Toher, S. Curtarolo, J. Maria, D. Brenner, Charge compensation and electrostatic transferability in three entropy-stabilized oxides: results from density functional theory calculations, J. Appl. Phys. 120 (9) (2016), 095015, https://doi.org/10.1063/1.4962135.
- [19] D. Bérardan, S. Franger, D. Dragoe, A. Meena, N. Dragoe, Colossal dielectric constant in high entropy oxides, Phys. Status Solidi - Rapid Res Lett. 10 (4) (2016) 328–333, https://doi.org/10.1002/pssr.201600043.
- [20] M. Biesuz, L. Spiridigliozzi, G. Dell'Agli, M. Bortolotti, V. Sglavo, Synthesis and sintering of (mg, co, ni, cu, zn)o entropy-stabilized oxides obtained by wet chemical methods, J. Mater. Sci. 53 (2018) 8074–8085, https://doi.org/10.1007/ s10853-018-2168-9.
- [21] D.R. Diercks, G.L. Brennecka, B.P. Gorman, C.M. Rost, J. Maria, Nanoscale compositional analysis of a thermally processed entropy-stabilized oxide via correlative tem and apt, Microsc. Microanal. 23 (2017) 1640–1641, https://doi. org/10.1017/S1431927617008868.
- [22] D. Bérardan, S. Franger, A.K. Meena, N. Dragoe, Room temperature lithium superionic conductivity in high entropy oxides, J. Mater. Chem. A 4 (24) (2016) 9536–9541, https://doi.org/10.1039/c6ta03249d.
- [23] B.H. Toby, R.B. VonDreele, GSAS-II: the genesis of a modern open-source all purpose crystallography software package, J. Appl. Crystallogr. 2 (46) (2013) 544–549, https://doi.org/10.1107/S0021889813003531.

- [24] B.H. Toby, R.B.V. Dreele, GSAS-ii: the genesis of a modern open-source all purpose crystallography software package, J. Appl. Crystallogr. 46 (2) (2013) 544–549, https://doi.org/10.1107/S0021889813003531.
- [25] Book of Standards. Vol.03-01. E112-13 standard test methods for determining average grain size. ASTM. 2013. DOI: 10.1520/E0112-13. https://www.astm. org/e0112-13.html.
- [26] K.W.E.C.A. Schneider, W.S. Rasband, Nih image to image; 25 years of image analysis, Nat. Methods 9 (7) (2012) 671–675, https://doi.org/10.1038/ nmeth.2089.
- [27] F.I.K. Momma, Vesta 3 for three-dimensional visualization of crystal, volumetric and morphology data, J. Appl. Crystallogr. 44 (2011) 1272–1276.
- [28] Y-M Chang, D.P. Birnie, W. David Kingery, Physical Ceramics: Principles for Ceramic Science and Engineering, Wiley, New York, 1997.
- [29] K. Gann, Phase Stability, Sintering, and Electrical Properties of the (Mg,Ni,Co,Cu, Zn)O Entropy Stabilized Oxide System. (Ph.D. thesis), Colorado School of Mines, 2018
- [30] A. Moulson, J. Herbert, Electroceramics: Materials, Properties. Applications, Second Edition, John Wiley Sons Ltd., 2003.
- [31] W. Kingery, H. Bowen, D. Uhlmann, Introduction to Ceramics, second ed., Wiley,, 1976.